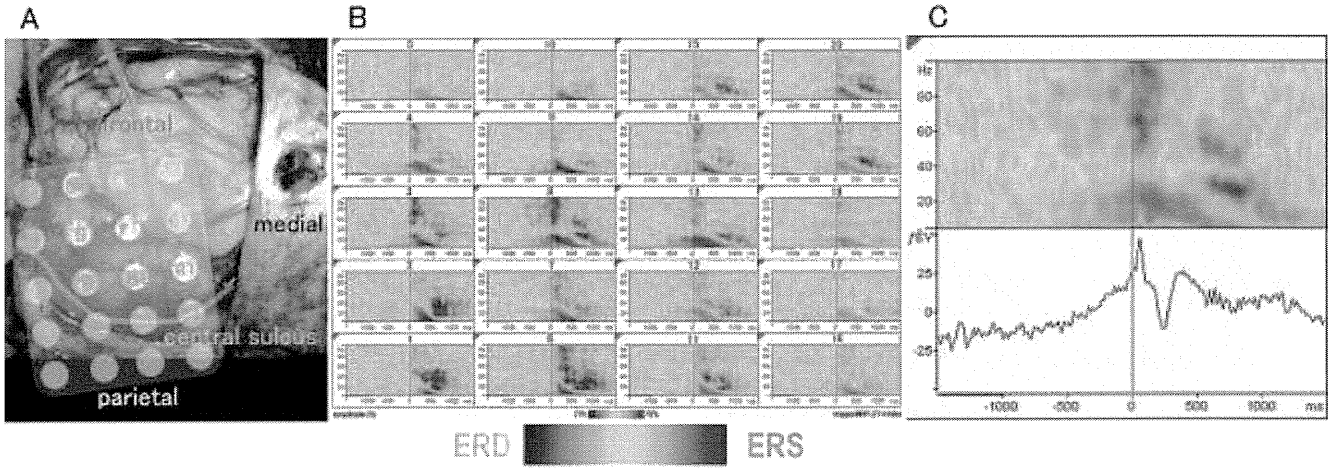

A. Electrode configuration on the brain. B. Time-frequency spectrograms of the grid electrodes. ERS in the γ band is focally distributed, whereas ERD in the α and β bands is broadly distributed. C. A time-frequency spectrogram (upper) and a cortical potential (lower) of electrode 8.
Fig. 1 Cerebral oscillatory changes recorded from brain surface grid electrodes.

2.2 Conventional methods for MEG analyses

Averaged waveforms, isomagnetic fields, and equivalent current dipoles (ECDs) are conventional methods for MEG analyses. Averaged waveforms are used to detect weak neuromagnetic activities by improving signal-to-noise ratio by averaging time-locked signals. They are appropriate for detecting relatively short latency activities less than several hundred milliseconds. Isomagnetic fields estimate rough localization of an electric current generator from the distribution of inflow and outflow magnetic fields. An ECD estimates the localization, magnitude and direction of an electric current generator quantitatively as an electric dipole equivalent to the distribution of inflow and outflow magnetic fields based on the Biot-Savart law. These methods enable us to grasp neural activities based on relatively simple principles, while they have several disadvantages. First, for example, when we detect evoked responses to specific stimuli using averaged waveforms, averaging process improves signal-to-noise ratio of the short latency responses. In contrast, high frequency components tend to be lost in the late latency, because the phases of neural responses in the latency might vary from a stimulus to a stimulus, which is a typical characteristic of biological responses. Second, an ECD estimates an electric current generator as a point. However, higher brain functions such as language and cognitive functions activate multiple brain areas simultaneously. ECD has some difficulty in estimating such complex spatial distribution.

2.3 Adaptive beamformer

To overcome these issues, various methods to estimate complex spatial distribution of neural activities have been introduced. Adaptive beamformer is a spatial noise filtering method and it is used to estimate complex spatial distribution of neural activities from unaveraged MEG signals [6]. Compared with conventional methods, adaptive beamformer takes advantages as follows: 1) high spatial resolution by statistical spatial filtering, 2) ability to elucidate the activities in the high frequency bands and in the late latency without averaging.

Adaptive beamformer assumes the matrix of each voxel within region of interest (ROI) as a virtual sensor array, and estimates source power for each voxel by minimizing signal power due to all other sources. The spatiotemporal MEG signal **M** can be written in matrix form:

$$\mathbf{M} = [m_{ik}] \quad (1)$$

$$i = 1\sim M,\ k = 1\sim K$$

M: number of sensors

K: number of time samples

m_{ik} is a function of the current **J** throughout the head volume Ω:

$$m_{ik} = \int_{\Omega} \mathbf{J}_k(\mathbf{r}) \bullet \mathbf{G}_i(\mathbf{r}) dr^3 + n_{ik} \quad (2)$$

where Green's functions G are used to represent the sensitivity of each sensor to current flow, and n is the instantaneous noise at sensor i. The sensor variance is

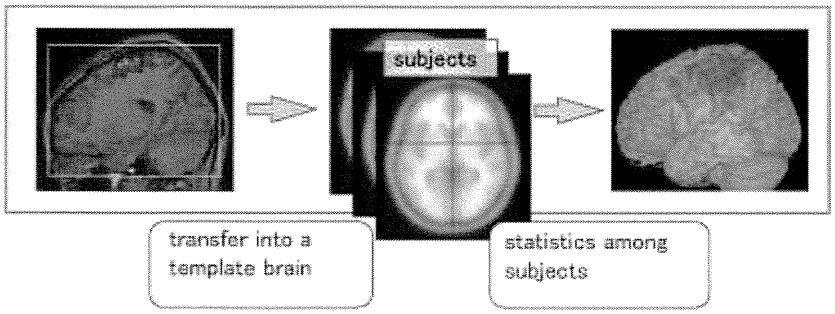

Fig. 2 A conceptual diagram of group analyses

represented by diagonal matrix $\sum$:

$$\sum = \begin{bmatrix} \sigma_1^2 & & 0 \\ & \ddots & \\ 0 & & \sigma_M^2 \end{bmatrix} \quad (3)$$

The source power estimate S_θ is:

$$S_\theta^2 = [\mathbf{H}_\theta^T \mathbf{M}]^2 \quad (4)$$

H: a vector of M beamforming coefficients

M: the signal space vector

θ : the target within brain.

The source noise variance is estimated:

$$\sigma_\theta^2 = \mathbf{H}_\theta^T \sum \mathbf{H}_\theta \quad (5)$$

Two additional constraints are required for solution of the beamforming coefficients. First, power S must be a measure of source and not signal:

$$\mathbf{H}_\theta^T \mathbf{G}_\theta \equiv 1 \quad (6)$$

Second, uncorrelated noise will appear in the source power estimate of equation 5. This constraint sets an upper limit on the noise:

$$\sigma_\theta \leq \xi_\theta \quad (7)$$

The beamformer coefficients are computed by minimizing source power (equation 4):

$$S_\theta^2 = \mathbf{H}_\theta^T \mathbf{C} \mathbf{H}_\theta \quad (8)$$

min **H**

C: the covariance matrix.

Thus, the source power estimate solution becomes:

$$S_\theta^2 = [\mathbf{G}_\theta^T [\mathbf{C} + \mu \sum]^{-1} \mathbf{G}_\theta]^{-1} \quad (9)$$

μ : a Backus-Gilbert regularization parameter.

2.4 Group analyses

We introduced group analyses to obtain common brain activities among subjects eliminating inter-individual difference (Fig. 2) [7].

Group statistical maps are generated by normalizing the individual results to standard space and then combining these results across subjects for each frequency band. First, each individual's anatomical MRI is resliced to the same orientation and position as the beamforming MEG results and statistical parametric mapping is used to find the transformation matrix from this functional space into the Montreal Neurological Institute (MNI) template. The transformation matrix is then applied to each of the beamforming MEG results in each frequency band, and for each subject. A permutation test is used to generate group statistical maps over each voxel in the standard brain using statistical non-parametric mapping (SnPM; Wellcome Department of Imaging Neuroscience, London, UK). Analysis at the voxel level was performed using a pseudo-T-statistic incorporating variance smoothing with a Gaussian kernel of width 8mm. These group statistical maps were then thresholded at $p < 0.001$ (corrected), and superimposed on the MNI template brain using mri3dX (CUBRIC, Cardiff, UK).

2.5 Neural decoding

Neural decoding is a method to infer the content of behavior or cognition from brain signals alone. Progress of functional brain researches has enabled us to neural decoding. Various methods are used for neural decoding. Here, we show a support vector machine (SVM) [8], which we use to decode neuromagnetic signals during upper hand and arm movements in our study [9].

An SVM is a learning machine which is often used for pattern recognition. It constructs a hyperplane or set of hyperplanes in a high- or infinite-dimensional

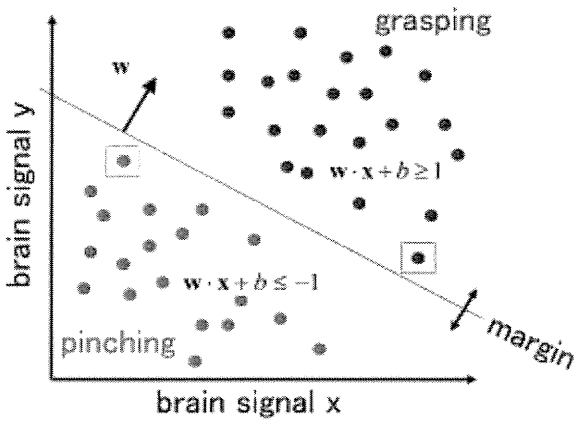

Fig. 3 A conceptual diagram of a support vector machine

space, which can be used for classification, regression, or other tasks. Intuitively, a good separation is achieved by the hyperplane that has the largest distance to the nearest training data point of any class, so-called functional margin, since in general the larger the margin the lower the generalization error of the classifier (Fig 3). An SVM takes a set of input data and predicts, for each given input, which of multiple possible classes forms the input, making it a non-probabilistic classifier. Given a set of training examples, each marked as belonging to one of multiple categories, an SVM training algorithm builds a model that assigns new examples into one category.

An SVM model is a representation of the examples as points in space, mapped so that the examples of the separate categories are divided by a clear gap that is as wide as possible. New examples are then mapped into that same space and predicted to belong to a category based on which side of the gap they fall on.

3. Neuromagnetic imaging of cerebral oscillatory changes

3.1 Somatosensory processing

Typical neuromagnetic somatosensory responses are observed when we stimulate major peripheral nerves of the body. We measured neuromagnetic responses using a whole head type axial gradiometer equipped with 64 SQUID sensors. Fig 4 shows the averaged waveforms of the somatosensory responses of all 64 SQUID sensors for 100 electrical stimuli to the right median nerve at the wrist in a healthy subject. Clear responses are observed in 20 ms, 26 ms, 39ms and 51 ms after the stimuli. Isomagnetic field maps show clear inflow and outflow of neuromagnetic fields. A current dipole equivalent to the magnetic field at 20 ms after the stimuli is localized just in the contralateral postcentral gyrus. The postcentral gyrus is well known as the primary somatosensory area, where somatosensory processing such as touch and vibration sensation of the body.

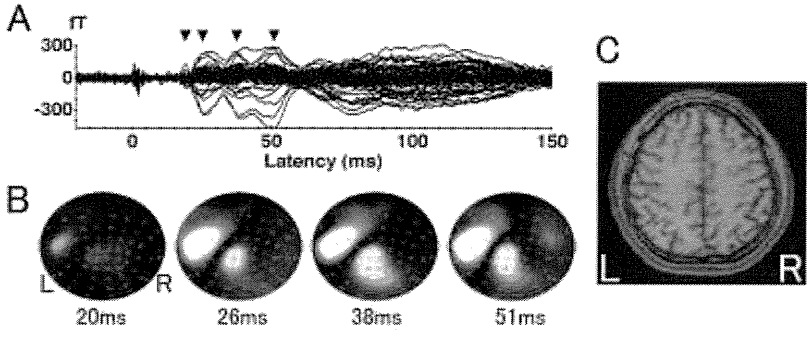

Neuromagnetic responses to the right median nerve electrical stimulation
A. Averaged waveforms
B. Isomagnetic fields
Inflows are indicated in red and outflows in blue.
C. An equivalent current dipole
Fig. 4 Standard MEG analyses

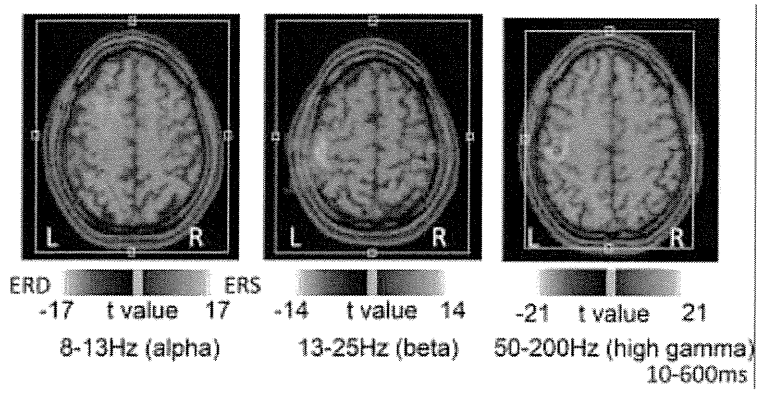

Fig. 5 Cerebral oscillatory changes during somatosensory stimulation revealed by beamforming MEG analyses

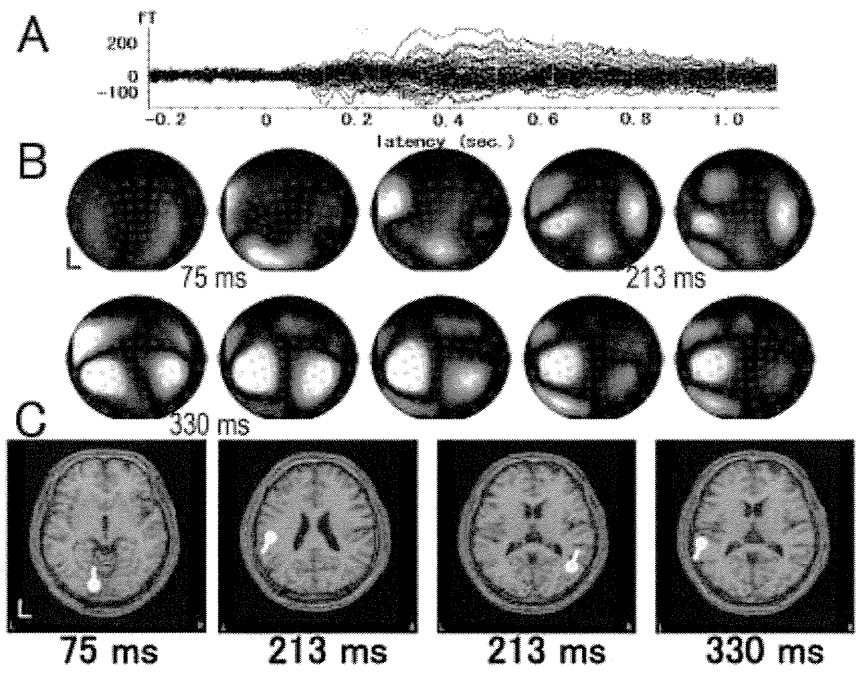

A. Averaged waveforms
B. Isofield maps
C. Equivalent current dipoles (ECDs)
Compared to somatosensory responses, averaged waveforms have late latency components and isofield maps indicate complex inflow and outflow distribution. Single ECD represents only part of the complex neuromagnetic fields. However, multiple ECD analyses failed to localize stable ECDs with sufficient goodness of fit.
Fig. 6 Neuromagnetic responses during silent reading.

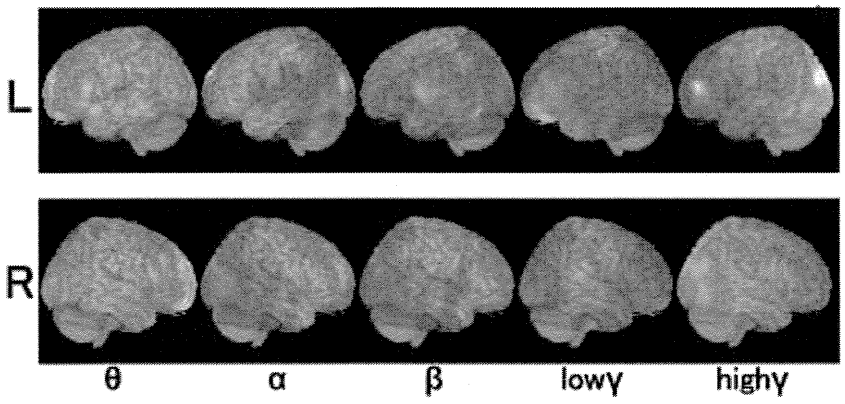

Beamforming MEG group analyses well represent frequency-dependent complex spatial distribution of cerebral oscillatory changes during silent reading. ERDs in the α band distributed in the receptive language area, whereas ERDs in the low γ band distributed in the expressive language area.
Fig. 7 Spatial distribution of cerebral oscillatory changes during silent reading revealed by beamforming MEG group analyses for 14 healthy right-handed subjects.

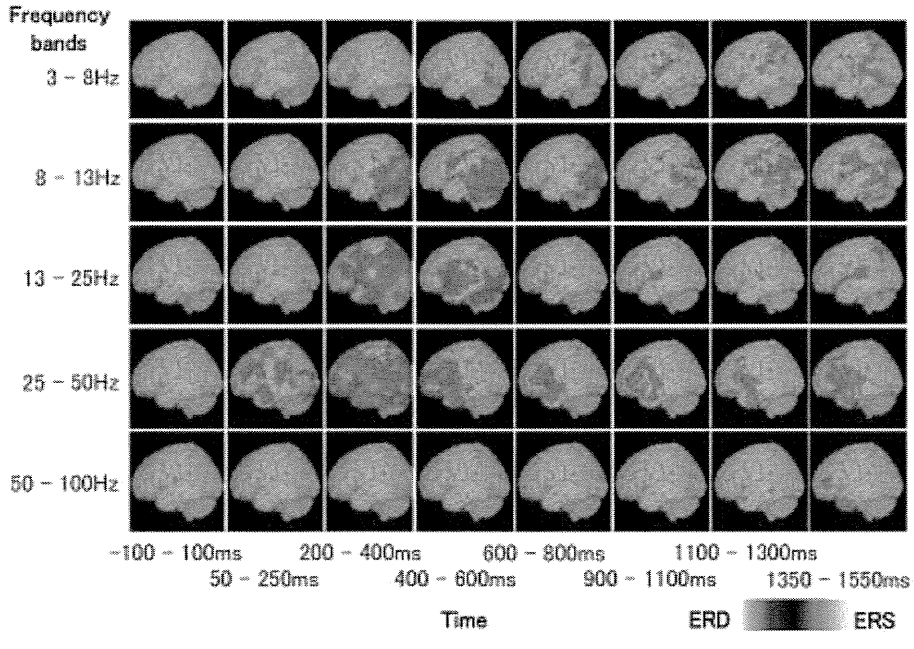

Sliding time window analyses of beamforming MEG reveal the temporal profiles of cerebral oscillatory changes during silent reading. Note that transient θ ERS precedes α to low γ ERDs. High γ ERS was found in the occipital lobe, which reflects visual processing.
Fig. 8 Time course of spatial distribution of cerebral oscillatory changes during silent reading revealed by beamforming MEG group analyses.

Beamformer analyses provide us with additional information about spatiotemporal distribution of neural processing. Beamformer analyses show the distributed ERS in the contralateral somatosensory area in the high γ band (50 – 200Hz) as well as the ERDs in the bilateral somatosensory areas in the α (8 – 13Hz) and β (13 – 25 Hz) bands (Fig 5) [10]. These ERDs and ERS are suggested to reflect inhibitory and excitatory neural activities related to somatosensory processing.

3.2 Language processing

Compared to somatosensory processing, neuromagnetic responses to linguistic stimuli are more complex. We use a silent reading task to avoid the noise contamination due to muscle contraction during phonation. A 3-character hiragana word was presented on a display for 3 seconds. Subjects are instructed to silently read the words once as soon as the words were presented. A total of 100 words were presented serially every 6 seconds. Fig 6A shows the averaged waveforms of neuromagnetic responses of all 64 SQUID sensors for visually-presented hiragana words in a healthy subject. They have later latency components and isofield maps indicate more complex inflow and outflow distribution than those of somatosensory processing (Fig 6B). Single ECD analyses managed to localize an ECD until 330ms, but represented only part of the complex neuromagnetic fields. Multiple ECD analyses failed to localize stable ECDs with sufficient goodness of fit.

Beamformer analyses provide us with complex spatial distribution of cerebral oscillatory changes during silent reading. Fig 7 shows the result of group analysis for 14 healthy right-handed subjects. It is noteworthy that the spatial distribution is dependent on the frequency bands of the oscillatory changes. ERDs in the α band distributed in the posterior (receptive) language area, whereas ERDs in the low γ band distributed in the frontal (expressive) language area [7]. In addition, we found that the left and right lateralization of ERD in the frontal area

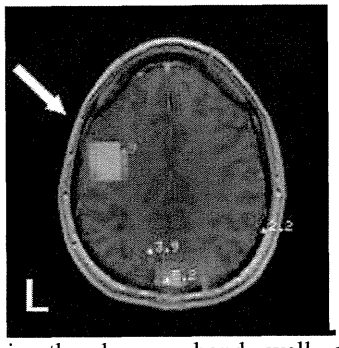

ERD is indicated by blue color area.

Fig. 9 Language dominance estimated by left and right lateralization of ERD in the frontal area in the low γ band

in the low γ band well corresponds to language dominance [11]. Using this property, we established the method to evaluate language dominance noninvasively with beamforming MEG analyses. Compared to the standard but invasive method for language dominance (the Wada test) which requires the injection of anesthetic agents intra-arterially at the carotid artery, the consistency is approximately 85% [7]. Beamforming MEG analysis is considered to be an alternative to the Wada test in selected cases. Fig. 9 shows an example of language dominance evaluated by this method.

Sliding time window analyses of beamforming MEG revealed the temporal profiles of cerebral oscillatory changes during silent reading (Fig 8) [12]. We found that the transient ERS first occurred in the occipital visual area, then in the temporo-occipital language areas, and finally propagated to the frontal language areas. This transient θ (8 – 13Hz) ERS was followed by α ERDs in the temporo-occipital language areas and low γ ERDs in the frontal language areas. High γ ERS was found in the occipital lobe, which reflects visual processing. It seems that transient θ ERS reflects serial processing while α and low γ ERDs reflect parallel neural processing.

4. Neural decoding of upper limb movements using single trial neuromagnetic signals

We investigated neural decoding of upper limb movements using single trial neuromagnetic signals.

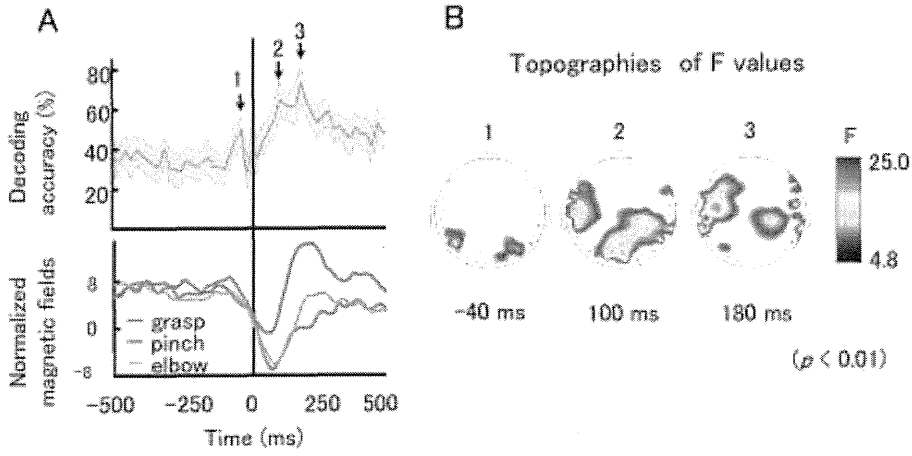

A. Temporal profiles of averaged waveforms of normalized magnetic fields and decoding accuracy in a representative subject.

B. Topography of F values among three movements

Fig. 10 Neural decoding of upper limb movements using single trial neuromagnetic signals.

Neuromagnetic activities were recorded in 9 healthy subjects during 3 types of unilateral upper limb movements. The movement types were inferred by a SVM. A one-way analysis of variance (ANOVA) was performed to reveal the spatiotemporal differences in the magnetic fields among the three movements. Significant F values in all MEG channels were calculated using the same parameters used for calculating the time course of the decoding accuracy. The topographies of the F values were delineated on a map of MEG sensors to determine which channels exhibited significant differences in neuromagnetic activities among movements.

The movement types were successfully predicted with an average accuracy of 66 ± 10% (chance level: 33.3%) using neuromagnetic activity during a 400-ms interval (-200 ms to 200 ms from movement onsets) [13]. Fig 10A shows the temporal profiles of averaged waveforms of normalized magnetic fields and decoding accuracy in a representative subject. Three peaks of decoding accuracy were found corresponding to the peaks of averaged waveforms of neuromagnetic fields. Topography of F values showed that high F values distributed over the parietal and sensorimotor areas (Fig 10B). The decoding accuracy was significantly correlated with amplitude of normalized neuromagnetic fields [9].

Our results indicate that the three types of unilateral upper limb movement can be inferred with high accuracy by detecting differences in movement-related brain activity in the parietal and sensorimotor areas.

5. Summary

We reviewed the recent progress in our MEG research on clinical application regarding functional neuroimaging and neural decoding using neuromagnetic recordings. Beamforming MEG analyses provide us with frequency-dependent spatiotemporal information about the cerebral oscillatory changes related to not only somatosensory processing but also language processing. Language dominance is able to be evaluated using laterality of the low γ ERD in the frontal area. Neuromagnetic signals of the unilateral upper movements are able to be decoded using a SVM.

Acknowledgments

This work was supported in part by Grants-in-Aid for Scientific Research (22390275, 23390347, 24000012, 24650106) from JSPS, by Health and Labour Sciences Research Grants (23100101) and by the Strategic Research Program for Brain Sciences of MEXT.

References

[1] ZN. Lu et al ed., Magnetic source imaging of the human brain, Lawrence Erlbaum Associates, Publishers, New Jersey, 2003.

[2] H. Stefan, C. Hummel, G. Scheler, A. Genow, K. Druschky, C. Tilz, M. Kaltenhauser, R. Hopfengartner, M. Buchfelder and J. Romstock, "Magnetic brain source imaging of focal epileptic activity: a synopsis of 455 cases," Brain : a journal of neurology, vol.126, no.Pt 11, pp.2396-2405, Nov, 2003.

[3] N. Birbaumer and L.G. Cohen, "Brain-computer interfaces: communication and restoration of movement in paralysis," J Physiol, vol.579, no.Pt 3, pp.621-636, Mar 15, 2007.

[4] G. Pfurtscheller and A. Aranibar, "Event-related cortical desynchronization detected by power measurements of scalp EEG," Electroencephalogr Clin Neurophysiol, vol.2, pp.817-826, 1977.

[5] G. Pfurtscheller, "Event-related synchronization (ERS): an electrophysiological correlate of cortical areas at rest," Electroencephalogr Clin Neurophysiol, vol.83, pp.62-69, 1992.

[6] S.E. Robinson and J. Vrba: Functional neuro-imaging by synthetic aperture magnetometry (SAM), in *Recent Advances in Biomagnetism*, T Yoshimoto et al (Eds.), pp.302-305, Tohoku Univ. Press, 1999.

[7] M. Hirata, T. Goto, G. Barnes, Y. Umekawa, T. Yanagisawa, A. Kato, S. Oshino, H. Kishima, N. Hashimoto, Y. Saitoh, N. Tani, S. Yorifuji and T. Yoshimine, "Language dominance and mapping based on neuromagnetic oscillatory changes: comparison with invasive procedures," J Neurosurg, vol.112, no.3, pp.528-538, Mar, 2010.

[8] Y. Kamitani and F. Tong, "Decoding the visual and subjective contents of the human brain," Nat Neurosci, vol.8, no.5, pp.679-685, May, 2005.

[9] H. Sugata, T. Goto, M. Hirata, T. Yanagisawa, M. Shayne, K. Matsushita, T. Yoshimine and S. Yorifuji, "Movement-related neuromagnetic fields and performances of single trial classifications," Neuroreport, vol.23, no.1, pp.16-20, 2012.

[10] M. Hirata, A. Kato, M. Taniguchi, H. Ninomiya, D. Cheyne, S.E. Robinson, M. Maruno, E. Kumura, R. Ishii, N. Hirabuki, H. Nakamura and T. Yoshimine, "Frequency-dependent spatial distribution of human somatosensory evoked neuromagnetic fields," Neurosci Lett, vol.318, pp.73-76, 2002.

[11] M. Hirata, A. Kato, M. Taniguchi, Y. Saitoh, H. Ninomiya, A. Ihara, H. Kishima, S. Oshino, T. Baba, S. Yorifuji and T. Yoshimine, "Determination of language dominance with synthetic aperture magnetometry: comparison with the Wada test," Neuroimage, vol.23, pp.46-53, 2004.

[12] T. Goto, M. Hirata, Y. Umekawa, T. Yanagisawa, M. Shayne, Y. Saitoh, H. Kishima, S. Yorifuji and T. Yoshimine, "Frequency-dependent spatiotemporal distribution of cerebral oscillatory changes during silent reading: a magnetoencephalograhic group analysis," NeuroImage, vol.54, no.1, pp.560-567, Jan 1, 2011.

[13] H. Sugata, T. Goto, M. Hirata, T. Yanagisawa, M. Shayne, K. Matsushita, T. Yoshimine and S. Yorifuji, "Neural decoding of unilateral upper limb movements using single trial MEG signals," Brain Res, Jun 8, 2012.

Masayuki Hirata, B.S., M.S. and M.D. and Ph.D. graduated from Faculty of Engineering, The University of Tokyo in 1985 and Osaka University Medical School in 1994. Board-certified neurosurgeon specialized in functional neurosurgery. He was promoted to a Specially-Appointed Associate Professor, Dept. of Neurosurgery, Osaka University Medical School serving as a leader of neural engineering group.

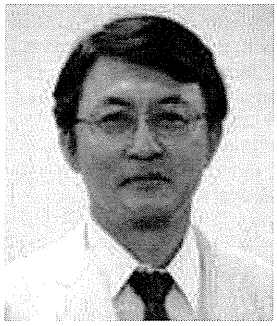

Toshiki Yoshimine, M.D., Ph.D. graduated from Osaka University Medical School in 1975. Board-certified neurosurgeon, specialized in brain tumor and epilepsy surgery. He is a Director, Japan Neurosurgical Society, and Neurotrauma Committee Member, World Federation of Neurosurgical Societies (WFNS). He has been a research fellow in Mayo Clinic in 1980-1983, a visiting professor in University of Mainz in 1995. He currently serves as Professor and Chairman, Dept. of Neurosurgery, Osaka University Medical School and Director, Medical Center for Translational Research, Osaka University Hospital.

Behavioural Neurology 00 (2013) 1–6
DOI 10.3233/BEN-110249
IOS Press

Possible roles of the dominant uncinate fasciculus in naming objects: A case report of intraoperative electrical stimulation on a patient with a brain tumour

Keiko Nomura[a], Hiroaki Kazui[a,*], Hiromasa Tokunaga[a], Masayuki Hirata[b], Tetsu Goto[b], Yuko Goto[b], Naoya Hashimoto[b], Toshiki Yoshimine[b] and Masatoshi Takeda[a]
[a]*Department of Psychiatry, Osaka University Graduate School of Medicine, Suita-city, Osaka, Japan*
[b]*Department of Neurosurgery, Osaka University Graduate School of Medicine, Suita-city, Osaka, Japan*

Abstract. How the dominant uncinate fasciculus (UF) contributes to naming performance is uncertain. In this case report, a patient with an astrocytoma near the dominant UF was given a picture-naming task during intraoperative electrical stimulation in order to resect as much tumourous tissues as possible without impairing the dominant UF function. Here we report that the stimulations with the picture-naming task also provided some insights into how the dominant UF contributes to naming performance. The stimulation induced naming difficulty, verbal paraphasia, and recurrent and continuous perseveration. Moreover, just after producing the incorrect responses, the patient displayed continuous perseveration even though the stimulation had ended. The left UF connects to the inferior frontal lobe, which is necessary for word production, so that the naming difficulty appears to be the result of disrupted word production caused by electrical stimulation of the dominant UF. The verbal paraphasia appears to be due to the failure to select the correct word from semantic memory and the failure to suppress the incorrect word. The left UF is associated with working memory, which plays an important role in recurrent perseveration. The continuous perseveration appears to be due to disturbances in word production and a failure to inhibit an appropriate response. These results indicate that the dominant UF has multiple roles in the naming of objects.

Keywords: Left uncinate fasciculus, naming objects, awake surgery, intraoperative electrical stimulation, low-grade astrocytoma

1. Introduction

The uncinate fasciculus (UF) is a white matter tract that connects the inferior frontal lobe with the anterior inferior temporal lobe [1]. A tumour resection study revealed that the left UF is essential for naming common objects [2]. Also, a diffusion tensor imaging (DTI) study found that demyelination and axonal injury of the left UF were associated with a decline in naming performance [3]. Although these two studies suggested that the left UF is associated with naming performance, they have a few shortcomings. In the tumour resection study, not only the left UF but also a part of the surrounding cortical regions was resected [2]. In the DTI study, the patients had temporal lobe epilepsy [3], which is likely to cause atypical language lateralization [4]. In addition, the DTI study did not assess whether the left UF was associated with symptoms that are related to naming deficits, such as paraphasia, perseverations, and speech arrest [3].

Intraoperative electrical stimulation inhibits the function of a restricted region of the brain [5], which makes it possible to observe real-time responses when the region has been functionally inhibited by the stimulation. There have been three reports on the ef-

*Corresponding author: Hiroaki Kazui, M.D., Ph.D., Department of Psychiatry, Osaka University Graduate School of Medicine, D3 2-2 Yamadaoka, Suita-city, Osaka, 565-0871, Japan. Tel.: +81 6 6879 3051; Fax: +81 6 6879 3059; E-mail: kazui@psy.med.osaka-u.ac.jp.

ISSN 0953-4180/13/$27.50

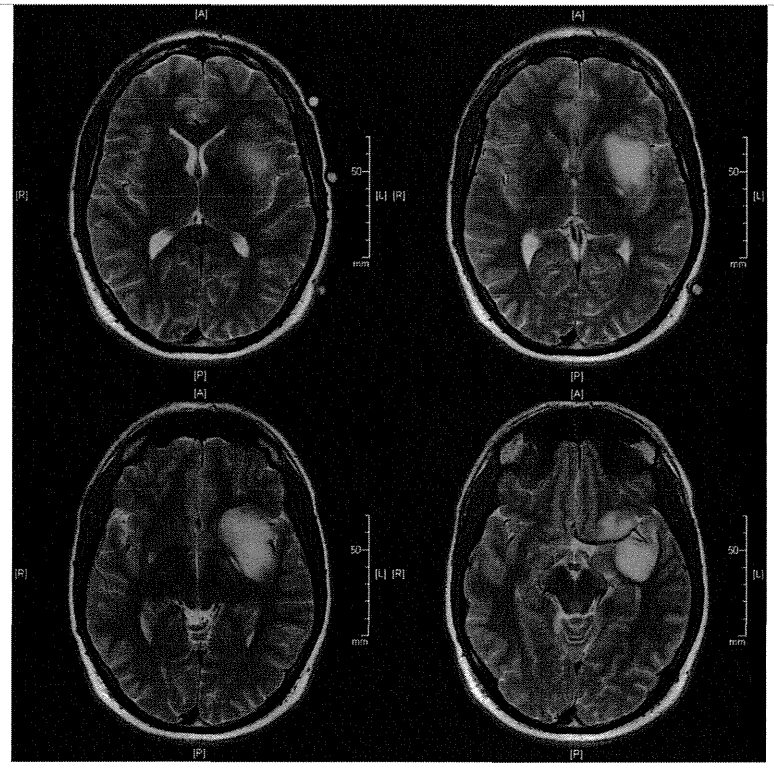

Fig. 1. Preoperative transaxial T1-weighted MR images showing a left frontotemporal low-grade astrocytoma, which involved the insula, temporal stem, and orbitofrontal cortex. A: anterior, P: posterior, R: right, L: left.

fects of intraoperative stimulation in the dominant UF, each reporting a different reaction: semantic paraphasia [6], phonetic paraphasia [2], and no language disturbance [7]. Although two of the studies [2,6] showed that the dominant UF is involved in naming performance, the types of naming errors differed between the two studies. Therefore, how the dominant UF is involved in naming performance is still uncertain. In the present study, intraoperative stimulation was used to assist in the resection of a tumour near the dominant UF. Here, we report that the patient showed multiple different symptoms related to naming objects during intraoperative stimulation of the dominant UF that provide some insights into how the dominant UF is involved in naming objects.

2. Methods

2.1. Patient

The patient was a 39-year-old Canadian man who had come to Japan in 2003 to teach English. He graduated from a college in Canada and spoke English as a first language. Following a motorbike accident, a routine computed tomography scan detected a tumour on the left insula, temporal stem, and orbitofrontal cortex. However, brain magnetic resonance (MR) images did not show contrast enhancement, so that the tumour was suspected to be benign and was followed up annually. Three years later, the tumour seemed to be larger, and was suspected to be a low-grade astrocytoma (Fig. 1). All preoperative and postoperative neuropsychological tests and an intraoperative naming test were performed in English. He was 100 percent right-handed as measured by the Edinburgh Handedness Inventory. According to the Magnetoencephalography and thiamylal sodium Wada Test with language tasks, his language functions were lateralised to the left hemisphere. The Wada Test also revealed that both hemispheres were involved in verbal memory. He experienced no seizure episodes or behavioural changes prior to the tumour resection. Written informed consent was obtained from the patient for publication of this report.

2.2. Preoperative cognitive performance

Preoperatively, the patient complained about mild word-finding difficulties only when he was talking with

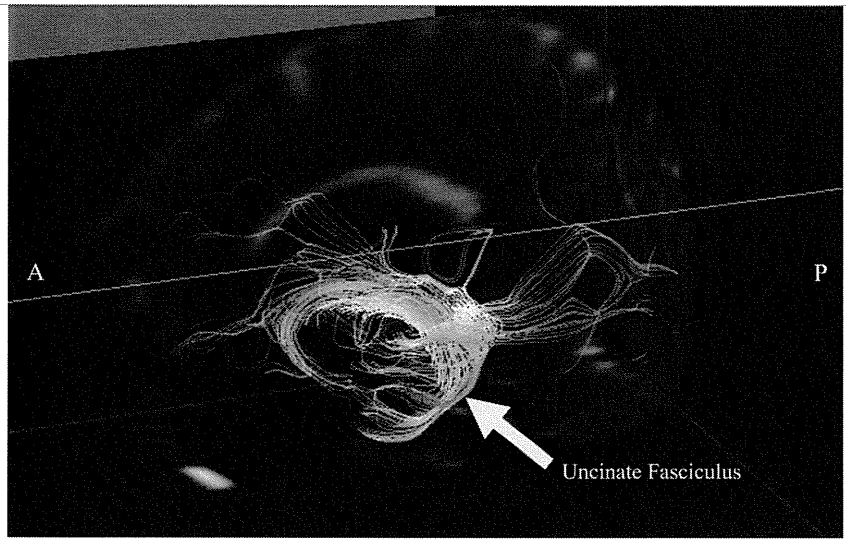

Fig. 2. Preoperative fibre tracking used to set the region of interest in the left temporal stem. The tract that is hooked at the left anterior temporal region was the left uncinate fasciculus (yellow arrow). The tract running backward is the left optic radiation. A: anterior, P: posterior.

native English speakers on business, but his colleagues did not make any remarks about it. He scored 30/30 on the Mini-Mental State Examination (MMSE). In the Western Aphasia Battery (WAB), he scored an aphasia quotient (AQ) of 99.6, a language quotient (LQ) of 99.8, and a cortical quotient (CQ) of 99.0, respectively. These results of the examinations indicated that his cognitive performance was not impaired.

2.3. *Preoperative magnetic resonance-diffusion tensor imaging data acquisition and processing*

Preoperatively, anatomical MR images and DTIs were acquired on a 3.0 Tesla MR whole-body imager (Signa VH/i, GE medical Systems, Milwaukee, WI, USA). Three-dimensional fibre tracking (FT) based on the DTI data was performed using Volume-One and dTV software (free software by Masutani, URL: http://www.ut-radiology.umin.jp/people/masutani/dTV.htm). The UF tractography was performed using a two-region of interest (ROI) method in the same way of a previous study [8]. The seed ROIs were placed in the anterior part of the UF in the coronal plane at the level of the anterior portion of the genu of the corpus callosum that was anterior to the anterior horn of the lateral ventricle. The target ROIs were placed in the white matter in the coronal plane at the most anterior part of the temporal stem. The colour-coded maps were employed to precisely and objectively place these ROIs into the UF tracts. To determine reconstructed coronal sections at the level of the genu of the corpus callosum, a reconstructed sagittal section of the colour-coded map was employed. Figure 2 shows the left UF with the FT images.

2.4. *Intraoperative electrical stimulation*

A Stryker Navigation System (Stryker, Kalamazoo, MI, USA) was used with 1.4 mm thin-slice sagittally sectioned MR images, which the FT had been superimposed on, for the navigation. After the main mass of the tumour was resected, electrical stimulation in combination with a picture-naming task was performed under local anaesthesia to determine whether additional tumorous tissue could be resected without impairing its function. The stimulation point abutted the posterior limb of the internal capsule and was very close to the left UF (Fig. 3). An Ojemann bipolar stimulator with 5 mm spaced tips was applied to deliver a biphasic current. The electrical stimulation was 6 mA. Each stimulation consisted of biphasic square wave pulses of 0.2 millisecond single phase duration at 50 Hz with the maximal train duration of five seconds. As Fig. 3 shows, we intermittently stimulated the same point at a distance of within 5 mm from the dominant UF. An electrical stimulation of 6 mA was shown to reach 5 mm from the stimulation point [9]. The electrocorticography activity was monitored to observe spontaneous or after-discharge spikes to minimise the risks of evoking a seizure by continued stimulation and to avoid the possibility of errors caused by the propagated effects of the current [2].

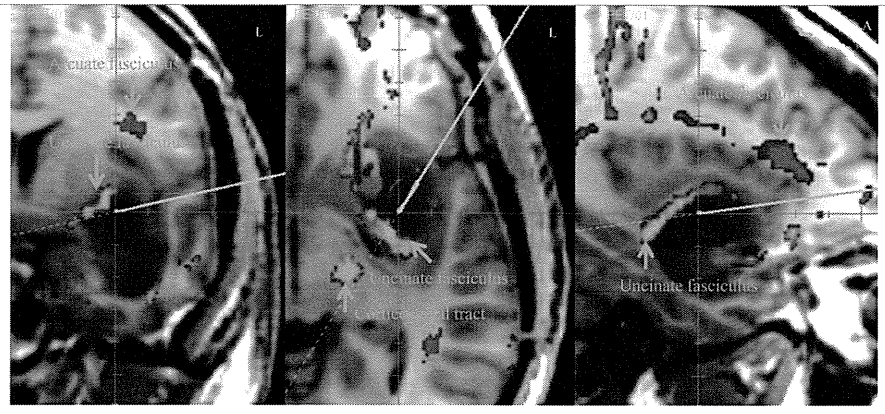

Fig. 3. Intraoperative neuronavigation pictures, in which the preoperative two-dimensional fibre tracking was projected on transaxial T1-weighted MR images (Left: a coronal image, Middle: a transaxial image, and Right: A sagittal image). The blue lines point to where the electrical stimulation with a picture-naming task was provided. L: left, A: anterior.

2.5. Picture-naming task

In the picture-naming task, the patient was asked to name a colour picture of an object that was on the computer screen beside his face. We prepared eight different colour pictures, which the patient could correctly name. The picture stimuli were presented repeatedly one after another in the following order: a clock, tire, banana, strawberry, pencil, umbrella, bicycle, and elephant. The picture-naming task was continuously performed while the dominant UF was being either stimulated or not stimulated. The patient was not informed when the dominant UF was being stimulated. The whole picture-naming task took approximately 10 minutes.

3. Results

3.1. Intraoperative electrical stimulation

We performed the picture-naming task eight times under the condition of stimulating the dominant UF. Among the eight times, the patient showed five incorrect responses. The patient stammered twice when he tried to name a picture of an umbrella and a banana respectively. The responses were considered as naming difficulty. When seeing a picture of a strawberry, the patient answered "fish", which was not in the picture stimuli. A fish and strawberry are not semantically interconnected, and the response was considered as verbal paraphasia. When the patient was shown a picture of an elephant, he answered "umbrella", which was shown two picture stimuli earlier. The response was considered as recurrent perseveration, which is an unintentional repetition of a preceding response when a new response following an interruption is expected to occur [10]. When asked a second time, he answered "umbrella" again. The response was considered as continuous perseveration, which is an inappropriate repetition of a preceding response without interruption [10]. Moreover, after producing the incorrect responses, the patient always gave the preceding incorrect response even though the stimulation had ended. The responses were considered as continuous perseveration. Except for the continuous perseveration, the patient did not produce any incorrect responses when not being stimulated.

3.2. Postoperative course

Since the stimulation of the dominant UF produced some naming and related disturbances, the neurosurgeons did not resect additional tissue of the dominant UF. The tumour resection was successful, so that neither chemotherapy nor radiotherapy was postoperatively given. One week after the operation, the patient scored 25/30 on the MMSE with scoring 2/5 on the serial 7's and scoring 1/3 on the recall. Regarding to his language performance, he scored the AQ of 100, the LQ of 100, and the CQ of 99.5, respectively. The patient did not show any naming difficulty, paraphasia, and perseveration. At six weeks after the operation, his MMSE score was completely back to 30/30, and he obtained a verbal memory index of 100, a visual memory index of 126, a general memory index of 106, an attention/concentration index of 102, and a delayed memory index of 105 in the Wechsler Memory Scale-Revised. Hence, his cognitive performances were not impaired by the tumour resection.

4. Discussion

When stimulating the dominant UF with the neuronavigation system during the picture-naming task, the patient displayed naming difficulty, verbal paraphasia, and recurrent and continuous perseveration. After producing the incorrect responses and after the stimulation had ended, the patient displayed continuous perseveration.

The findings of this report, in which the dominant UF stimulation caused some deteriorations of naming performance, are consistent with the results of previous tumour resection and DTI studies [2,3]. The left UF connects to the inferior frontal lobe, which is essential for word production [11]. Dysfunction of the dominant UF appears to be the cause of the naming difficulty.

The verbal paraphasia that we observed during the dominant UF stimulation is closely related to previous studies that found phonetic paraphasia and semantic paraphasia during the dominant UF stimulation with a picture-naming task [2,6]. The dominant anterior inferior temporal lobe, to which the UF connects [1], is involved in semantic memory that is information about the concept or meaning of words and objects [12,13]. Moreover, the UF is involved in verbal planning and suppression [14]. Hence, verbal perseveration should be caused by disturbances in selection of a semantically correct word and failures to suppress the inappropriate word.

Recurrent perseveration and continuous perseveration, which were induced by the dominant UF stimulation during the picture-naming task in this case, have not previously been reported to be caused by the dominant UF stimulation. Recurrent perseveration is initiated with an unsuccessful search in semantic memory for the correct word, and then a recently heard word can be selected from short-term memory [15]. A word, which has just been articulated, should be temporarily held in working memory (WM), with which the UF is associated [16]. In this case, the stimulation must have prevented the patient from retrieving a word from semantic memory, so that the patient incorrectly must have selected another word that had been recently articulated from WM.

Continuous perseveration was observed when motor output was disturbed [10] and was associated with a failure to inhibit an appropriate response [17]. Therefore, electrical stimulation of the dominant UF, which is involved in word production [11] and motor suppression [14], could produce continuous perseveration. Although it is unclear why continuous perseveration occurred just after switching off the stimulation, it was always observed after the patient produced the incorrect responses with the stimulation. The stimulation, which was enough to produce incorrect responses, might have produced continuous perseveration.

Several issues should be considered when generalising the findings of this case report. First, we need to acknowledge that we provided the picture-naming task only eight times under the condition of stimulating the UF, so that we were unable to examine whether the same incorrect responses can be observed repeatedly. Second, the tumour seemed to shift the UF medially, so that the UF may have not been placed in the expected anatomical region. Third, whenever the intraoperative neuronavigation system is employed, the possibility of an intraoperative brain shift should be considered [18, 19] because the brain shift may result in inaccuracy of stereotactic image guidance on the preoperatively acquired brain images [18] and may reduce reliability of the neuronavigation system [19]. However, the displacements of deep tumour margins or subcortical structures are not as pronounced as those of superficial or cortical structures [19,20]. Furthermore, experienced neurosurgeons identified the tumour and differentiated the brain structures including the cortices, white matter tracts, and deep brain structures based on their anatomical knowledge. Finally, we may have failed to depict the inferior occipitofrontal fasciculus (IOFF) independently from the UF because it is very difficult to distinguish these two regions in FT images [21]. Because the UF tractography method that we used has been shown to be reliable [8], we believe that we properly depicted the UF. In addition, because our stimulation point was very close to the UF (Fig. 3) and because the electric current we applied was enough to reach 5 mm from the stimulation point, the electrical stimulation must have reached the UF. Hence, we are confident that we properly stimulated the dominant UF instead of the IOFF.

In this case, stimulating the dominant UF caused several responses (naming difficulty, verbal paraphasia, and recurrent and continuous perseveration). These results indicate that the dominant UF is related to multiple roles in the naming of objects.

References

[1] Catani M, Howard RJ, Pajevic S, Jones DK. Virtual *in vivo* interactive dissection of white matter fasciculi in the human brain. *Neuroimage*. 2002; 17(1): 77-94.

[2] Papagno C, Miracapillo C, Casarotti A, Romero Lauro LJ, Castellano A, Falini A, Casaceli G, Fava E, Bello L. What is the role of the uncinate fasciculus? Surgical removal and proper name retrieval. *Brain.* 2011; 134(Pt 2): 405-414.

[3] McDonald CR, Ahmadi ME, Hagler DJ, Tecoma ES, Iragui VJ, Gharapetian L, Dale AM, Halgren E. Diffusion tensor imaging correlates of memory and language impairments in temporal lobe epilepsy. *Neurology.* 2008; 71(23): 1869-1876.

[4] Pataraia E, Simos PG, Castillo EM, Billingsley-Marshall RL, McGregor AL, Breier JI, Sarkari S, Papanicolaou AC. Reorganization of language-specific cortex in patients with lesions or mesial temporal epilepsy. *Neurology.* 2004; 63(10): 1825-1832.

[5] Duffau H, Capelle L, Sichez N, Denvil D, Lopes M, Sichez JP, Bitar A, Fohanno D. Intraoperative mapping of the subcortical language pathways using direct stimulations. An anatomofunctional study. *Brain.* 2002; 125(Pt 1): 199-214.

[6] Bello L, Gallucci M, Fava M, Carrabba G, Giussani C, Acerbi F, Baratta P, Songa V, Conte V, Branca V, Stocchetti N, Papagno C, Gaini SM. Intraoperative subcortical language tract mapping guides surgical removal of gliomas involving speech areas. *Neurosurgery.* 2007; 60(1): 67-80; discussion 80-62.

[7] Duffau H, Gatignol P, Moritz-Gasser S, Mandonnet E. Is the left uncinate fasciculus essential for language? A cerebral stimulation study. *J Neurol.* 2009; 256(3): 382-389.

[8] Yasmin H, Nakata Y, Aoki S, Abe O, Sato N, Nemoto K, Arima K, Furuta N, Uno M, Hirai S, Masutani Y, Ohtomo K. Diffusion abnormalities of the uncinate fasciculus in Alzheimer's disease: Diffusion tensor tract-specific analysis using a new method to measure the core of the tract. *Neuroradiology.* 2008; 50(4): 293-299.

[9] Kamada K, Todo T, Ota T, Ino K, Masutani Y, Aoki S, Takeuchi F, Kawai K, Saito N. The motor-evoked potential threshold evaluated by tractography and electrical stimulation. *J Neurosurg.* 2009; 111(4): 785-795.

[10] Sandson J, Albert ML. Varieties of perseveration. *Neuropsychologia.* 1984; 22(6): 715-732.

[11] Schuhmann T, Schiller NO, Goebel R, Sack AT. The temporal characteristics of functional activation in Broca's area during overt picture naming. *Cortex.* 2009; 45(9): 1111-1116.

[12] Damasio H, Grabowski TJ, Tranel D, Hichwa RD, Damasio AR. A neural basis for lexical retrieval. *Nature.* 1996; 380(6574): 499-505.

[13] Patterson K, Nestor PJ, Rogers TT. Where do you know what you know? The representation of semantic knowledge in the human brain. *Nat Rev Neurosci.* 2007; 8(12): 976-987.

[14] Hornberger M, Geng J, Hodges JR. Convergent grey and white matter evidence of orbitofrontal cortex changes related to disinhibition in behavioural variant frontotemporal dementia. *Brain.* 2011; 134(Pt 9): 2502-2512.

[15] Shindler AG, Caplan LR, Hier DB. Intrusions and perseverations. *Brain Lang.* 1984; 23(1): 148-158.

[16] Charlton RA, Barrick TR, Lawes IN, Markus HS, Morris RG. White matter pathways associated with working memory in normal aging. *Cortex.* 2010; 46(4): 474-489.

[17] Possin KL, Filoteo JV, Roesch SC, Zizak V, Rilling LM, Davis JD. Is a perseveration a perseveration? An evaluation of cognitive error types in patients with subcortical pathology. *J Clin Exp Neuropsychol.* 2005; 27(8): 953-966.

[18] Benveniste RJ, Germano IM. Correlation of factors predicting intraoperative brain shift with successful resection of malignant brain tumors using image-guided techniques. *Surg Neurol.* 2005; 63(6): 542-548; discussion 548-549.

[19] Reinges MH, Nguyen HH, Krings T, Hutter BO, Rohde V, Gilsbach JM. Course of brain shift during microsurgical resection of supratentorial cerebral lesions: Limits of conventional neuronavigation. *Acta Neurochir (Wien).* 2004; 146(4): 369-377; discussion 377.

[20] Hastreiter P, Rezk-Salama C, Soza G, Bauer M, Greiner G, Fahlbusch R, Ganslandt O, Nimsky C. Strategies for brain shift evaluation. *Med Image Anal.* 2004; 8(4): 447-464.

[21] Makris N, Papadimitriou GM, Sorg S, Kennedy DN, Caviness VS, Pandya DN. The occipitofrontal fascicle in humans: A quantitative, *in vivo*, DT-MRI study. *Neuroimage.* 2007; 37(4): 1100-1111.

Behavioral/Systems/Cognitive

Regulation of Motor Representation by Phase–Amplitude Coupling in the Sensorimotor Cortex

Takufumi Yanagisawa,[1,2,3]* Okito Yamashita,[4]* Masayuki Hirata,[1] Haruhiko Kishima,[1] Youichi Saitoh,[1,5] Tetsu Goto,[1] Toshiki Yoshimine,[1] and Yukiyasu Kamitani[3]

[1]Department of Neurosurgery and [2]Division of Functional Diagnostic Science, Osaka University Graduate School of Medicine, Osaka 565-0871, Japan, [3]Computational Neuroscience Laboratories and [4]Neural Information Analysis Laboratories, ATR (Advanced Telecommunications Research Institute International), Kyoto 619-0288, Japan, and [5]Department of Neuromodulation and Neurosurgery Office for University-Industry Collaboration, Osaka University, Osaka 565-0871, Japan

High-γ amplitude (80–150 Hz) represents motor information, such as movement types, on the sensorimotor cortex. In several cortical areas, high-γ amplitudes are coupled with low-frequency phases, e.g., α and θ (phase–amplitude coupling, PAC). However, such coupling has not been studied in the sensorimotor cortex; thus, its potential functional role has yet to be explored. We investigated PAC of high-γ amplitude in the sensorimotor cortex during waiting for and the execution of movements using electrocorticographic (ECoG) recordings in humans. ECoG signals were recorded from the sensorimotor cortices of 4 epilepsy patients while they performed three different hand movements. A subset of electrodes showed high-γ activity selective to movement type around the timing of motor execution, while the same electrodes showed nonselective high-γ activity during the waiting period (>2 s before execution). Cross frequency coupling analysis revealed that the high-γ amplitude during waiting was strongly coupled with the α phase (10–14 Hz) at the electrodes with movement-selective high-γ amplitudes during execution. This coupling constituted the high-γ amplitude peaking around the trough of the α oscillation, and its strength and phase were not predictive of movement type. As the coupling attenuated toward the timing of motor execution, the high-γ amplitude appeared to be released from the α phase to build a motor representation with phase-independent activity. Our results suggest that PAC modulates motor representation in the sensorimotor cortex by holding and releasing high-γ activity in movement-selective cortical regions.

Introduction

Neuronal oscillations in the sensorimotor cortex are characteristically modulated according to motor functions (Crone et al., 1998a; Cheyne et al., 2008; Miller et al., 2010; Muthukumaraswamy, 2010). Notably, the amplitudes of the high-γ (80–150 Hz; Canolty et al., 2006) and low-frequency bands, such as α (8–13 Hz) and β (13–30 Hz), have been shown to be important for motor functions. The high-γ amplitude represents motor information such as the type of movement and onset timing (Crone et al., 1998b; Yanagisawa et al., 2011). The amplitudes of the low-frequency bands have been attributed to cortical excitability, disengagement of task-irrelevant cortical areas, and maintenance of the status quo (Neuper and Pfurtscheller, 2001; Tamura et al., 2005; Engel and Fries, 2010; Saleh et al., 2010; Haegens et al., 2011b). However, it is not understood how these oscillations relate to each other and how their relationship affects the encoding of motor information.

It has been demonstrated that high-γ amplitude is modulated by the phase of low-frequency oscillations, such as θ (Canolty et al., 2006; Sirota et al., 2008; He et al., 2010) and α (8–13 Hz; Osipova et al., 2008), across multiple cortical and subcortical sites (Pineda, 2005; Cohen et al., 2009; Axmacher et al., 2010; Canolty and Knight, 2010; Voytek et al., 2010). Moreover, such phase–amplitude coupling (PAC) has a variety of functional roles in cortical processing, such as working memory (Axmacher et al., 2010) and sensory processing (Luo and Poeppel, 2007; Lakatos et al., 2008; Saleh et al., 2010). However, the functional role of PAC in the sensorimotor cortex during the preparation and execution of movements remains unknown. The main issues to be uncovered are as follows: (1) does PAC exist in the sensorimotor cortex during movement tasks and (2) how does the coupling affect the motor information represented by the high-γ amplitude?

To address these questions, we recorded electrocorticographic (ECoG) signals in the sensorimotor cortices of epilepsy patients while they executed three types of simple hand movements. First, using multichannel decoding and univariate statistical analyses, we show that the high-γ amplitudes during motor execution encode the information of movement type in a subset of electrodes. Next, we performed PAC analysis using the synchronization index (SI; Cohen, 2008) and found that high-γ activity during the waiting period was strongly coupled with a particular phase of the

Received June 20, 2012; revised Sept. 2, 2012; accepted Sept. 7, 2012.

Author contributions: T. Yanagisawa, O.Y., and Y.K. designed research; T. Yanagisawa, M.H., H.K., Y.S., T.G., and T. Yoshimine performed research; T. Yanagisawa and O.Y. analyzed data; T. Yanagisawa and Y.K. wrote the paper.

This work was supported in part by the Strategic Research Program for Brain Sciences of MEXT, KAKENHI (22700435, 23390347, 24650106, 24700419), the Ministry of Health, Labor and Welfare (18261201, 23100101), the Brain Science Foundation, and a contract with the National Institute of Information and Communications Technology.

This article is freely available online through the *J Neurosci* Open Choice option.

*T. Yanagisawa and O.Y. contributed equally to this work.

The authors declare no competing financial interests.

Correspondence should be addressed to Yukiyasu Kamitani, 2-2-2 Hikaridai, Seika, Soraku, Kyoto 619-0288, Japan. E-mail: kmtn@atr.jp.

DOI:10.1523/JNEUROSCI.2929-12.2012

 0270-6474/12/3215467-09$15.00/0

Table 1. Clinical profiles

Patient number	Age (years)/ sex	Diagnosis	Number of electrodes
1	34/F	R epilepsy	30
2	14/M	R epilepsy	15
3	22/F	R epilepsy	30
4	20/F	L epilepsy	20

F, Female; M, male; R, right; L, left.

α oscillation. On the basis of these analyses, we discovered a remarkable similarity between the spatial patterns of electrodes with movement selectivity at execution and those with strong PAC during waiting. We further examined the phase-conditioned high-γ amplitudes to characterize the dynamics of high-γ activity and the motor representation modulated by α oscillations.

Materials and Methods

Study subjects. Four patients with subdural electrodes participated in this study (1 male and 3 females; Table 1). All participants and their guardians were informed of the purpose and possible consequences of this study, and written informed consent was obtained. The present study was approved by the Ethics Committee of Osaka University Hospital.

Tasks. The experiments were performed at ~1 week after electrode placement in an electromagnetically shielded room. After >30 s of resting, during which time the patients were asked to stay quiet without moving, the patients selected and performed one of three types of movement every 5.5 s (Fig. 1*A*). The three types of movement consisted of grasping, pinching, and opening the hand. In each trial, the patient selected one of the three types of movement voluntarily. The movements were performed by the hand contralateral to the implanted electrodes. Three beep sounds were presented at 1 s intervals, and the patient was instructed to perform the movement immediately after the presentation of the third sound. The patient returned his or her hand to a resting position immediately after the movement. In the resting period, the patient relaxed his or her hand with slightly flexed joints. The patient repeated the trials ~120 times. Thus, each type of movement was performed ~40 times. In the control experiment, patients 1 and 2 performed a language task. After >30 s of resting, the patient was asked to voluntarily select and pronounce one of five Japanese vowels at an arbitrary timing.

ECoG recordings. In each patient, 15–30 planar-surface platinum grid electrodes (3 × 5, 4 × 5, or 5 × 6 array; Unique Medical) were placed over the sensorimotor cortex (Fig. 1*B*). The electrodes covered the precentral gyrus and postcentral gyrus centering around the "hand knob" for all patients. Most of the electrodes were placed on the precentral gyrus. The electrodes had a diameter of 3 mm and an interelectrode distance of 7 or 10 mm center to center. The location of the implanted electrodes was identified by standard neurosurgical techniques both anatomically and electrophysiologically. Preoperative structural magnetic resonance imaging (MRI) was performed on all patients using a 1.5-T or 3.0-T MRI scanner. Computed tomography (CT) scans were acquired postoperatively with subdural electrodes in place, clearly showing the position of the electrodes with respect to skull geometry. For an estimation of the position of the implanted electrodes through the use of BrainLAB, coregistration between the postoperative CT and preoperative MRI scans was obtained to create 3-dimensional brain renderings of the MRI volume overlaid with the coregistered CT volume for an initial estimate of the position of the electrodes. As necessary, these coregistrations were manually corrected using the position of the electrodes from intraoperative photographs.

Data collection and preprocessing. ECoG signals were measured using a 128-channel digital EEG system (EEG 2000; Nihon Koden Corporation) and digitized at a sampling rate of 1000 Hz. All subdural electrodes were referenced to a scalp electrode placed on the nasion. Before any further processing, channels with a low signal-to-noise ratio were identified and deleted. For the analysis, the ECoG signals were digitally re-referenced to a common average. The bandpass filter for the data analysis was set to 0.16–300 Hz. We analyzed ECoG signals time-locked to the third beep.

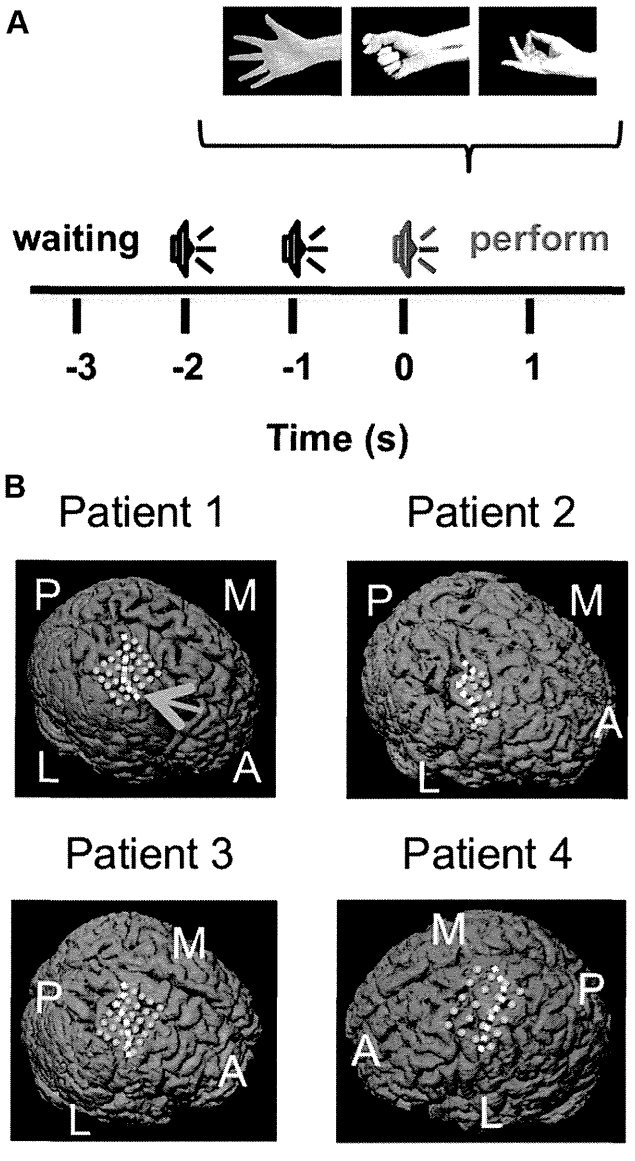

Figure 1. Task paradigm and location of the electrodes. ***A***, The patients selected and executed one of three movements in accordance with three sound cues. ***B***, The location of the implanted electrodes is indicated by the green circles on the 3-dimensional brain rendering of the MRI volume of each patient. The white dashed line indicates the location of the central sulcus. A, Anterior; L, lateral; M, medial; P, posterior.

Extraction of amplitude and phase features. The ECoG signals of each electrode were bandpass-filtered using a two-way least-squares finite impulse response filter (eegfilt.m from the EEGLAB toolbox). Then, the Hilbert transformation was performed on the filtered signals to obtain the complex-valued analytic signals of each frequency band, $X_\omega[t]$. Here, ω denotes the frequency band. The amplitude of each frequency band, $A_\omega[t]$, was calculated from the absolute value of the complex-valued signals using Equation 1. Similarly, the phase of each frequency band, $\phi_\omega[t]$, was calculated from the analytic phase of the complex-valued signals. The phase time series, $\phi_\omega[t]$, assumes values within $(0, 2\pi)$ radians with a cosine phase such that π radians correspond to the trough and 0 radians correspond to the peak

$$X_\omega[t] = A_\omega[t] \cdot \exp(i\,\phi_\omega[t]).$$

The amplitudes of each frequency band during the movement task were z-normalized using the mean and SD of the amplitudes during the 30 s

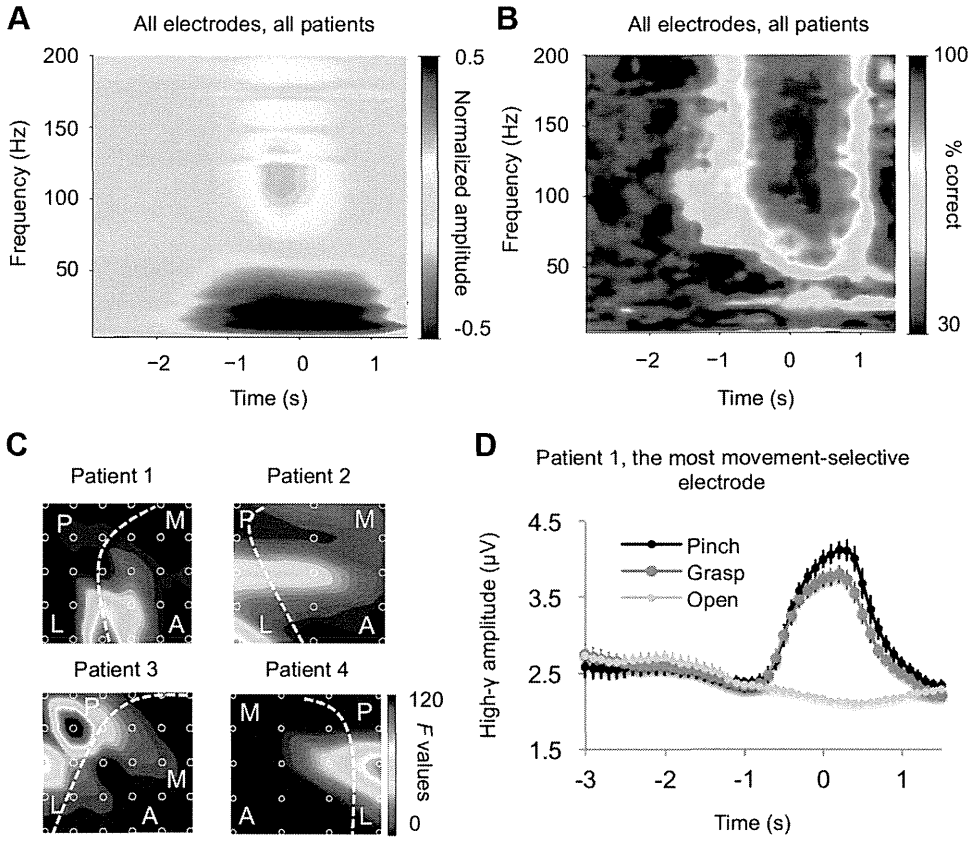

Figure 2. Motor representation by high-γ amplitude. ***A***, The normalized amplitude of each frequency band of 4 Hz width, which ranged from 2 to 200 Hz, was averaged across all trials and electrodes in all patients. The mean normalized amplitude of 1 s intervals centered at every 100 ms was color-coded at each frequency band and time. Time 0 corresponds to the sound cue to start the movement. ***B***, Movement classification was performed using the mean normalized amplitude of 1 s intervals at all electrodes for each frequency band, time, and patient (the number of input features for decoding was the number of electrodes of each patient). The percentage correct of the movement classification was averaged among the four patients and color-coded at each frequency and time. ***C***, The *F* value (one-way ANOVA) for the high-γ amplitude (80–150 Hz) of each electrode at time 0.5 s (0–1 s) among the movement types was color-coded to the location of the electrode for each patient. ***D***, The mean high-γ amplitude with a 95% confidence interval (95% CI) is shown for the three types of movement at a movement-selective electrode with a high *F* value of $p < 0.01$. The location of the electrode is indicated by the orange arrow in Figure 1*B*.

resting period before the movement task. For the main analysis, the normalized amplitudes were averaged over a 1 s time window, and the center of the window was shifted by 100 ms. For the phase-conditioned analysis, we divided the α phase into 6 intervals of 60° without overlaps: 0° ± 30°, 60° ± 30°, 120° ± 30°, 180° ± 30°, 240° ± 30°, and 300° ± 30°. In a 1 s time window, high-γ amplitudes were averaged within each phase interval.

PAC analysis. The SI was used to measure the strength of PAC between the high-γ amplitude and the low-frequency phases (Cohen, 2008). The high-γ amplitude was bandpass filtered by the low-frequency band ω using the finite impulse response filter to obtain $A_{\gamma\omega}[t]$. Then, the Hilbert transformation was applied to $A_{\gamma\omega}[t]$ to obtain the analytic phase $\phi_{\gamma\omega}[t]$. The synchronization index $SI_{\gamma\omega}[t]$ was obtained by

$$SI_{\gamma\omega} = \left| \frac{1}{n} \sum_{n=1}^{N} \exp(i(\phi_{\omega}(n) - \phi_{\gamma\omega}(n))) \right|,$$

where N is the number of time points during each 1 s time window. To determine whether the SI values were statistically significant, we calculated SI values using phase-shuffled data, in which the time series of the low-frequency phase was shuffled by permuting randomly partitioned segments. SI values were regarded as statistically significant if they were higher than those calculated using randomized phases with $p < 0.05$ (Student's *t* test).

Evaluation of selectivity to movement type. The motor information represented by the amplitudes of multiple electrodes was evaluated by decoding analysis using a linear support vector machine (Kamitani and Tong, 2005; Yanagisawa et al., 2009, 2011). Fivefold cross-validation was conducted in each patient to evaluate the generalization performance of the classifier (Breiman, 1996; Bengio and Grandvalet, 2004). For the decoding analysis using the PAC features, we used SI values and the phase differences between the α oscillation and the α component of the high-γ amplitude ($\phi_{\alpha}[t] - \phi_{\gamma\alpha}[t]$) averaged over a 1 s time window. For the evaluation of motor information in each electrode, the *F* value (one-way ANOVA statistic) was used to quantify how much the amplitude varied among the movement types.

Results

High-γ amplitudes represent movement types around the timing of motor execution at movement-selective cortical areas

To visualize the frequency components of the ECoG signals in the sensorimotor cortex associated with the hand movements, we first averaged the normalized amplitudes of each frequency band and their timing across all electrodes and trials in four patients (Fig. 2*A*). The averaged amplitudes showed that during motor execution, the ECoG signals increased in the high-γ range (80–150 Hz) and decreased in the α and β (8–30 Hz) range ($p < 0.01$, ANOVA). To reveal at which frequency and timing the specific movement types were represented, we performed decoding analysis using the amplitude pattern of all electrodes at a particular frequency and timing to predict one among three movement types. Decoding performance was evaluated on a trial-by-trial basis using a cross-validation procedure. As shown in Figure 2*B*, high decoding accuracy was found in the high-γ range around the timing of motor execution ($p < 0.01$, ANOVA). These results

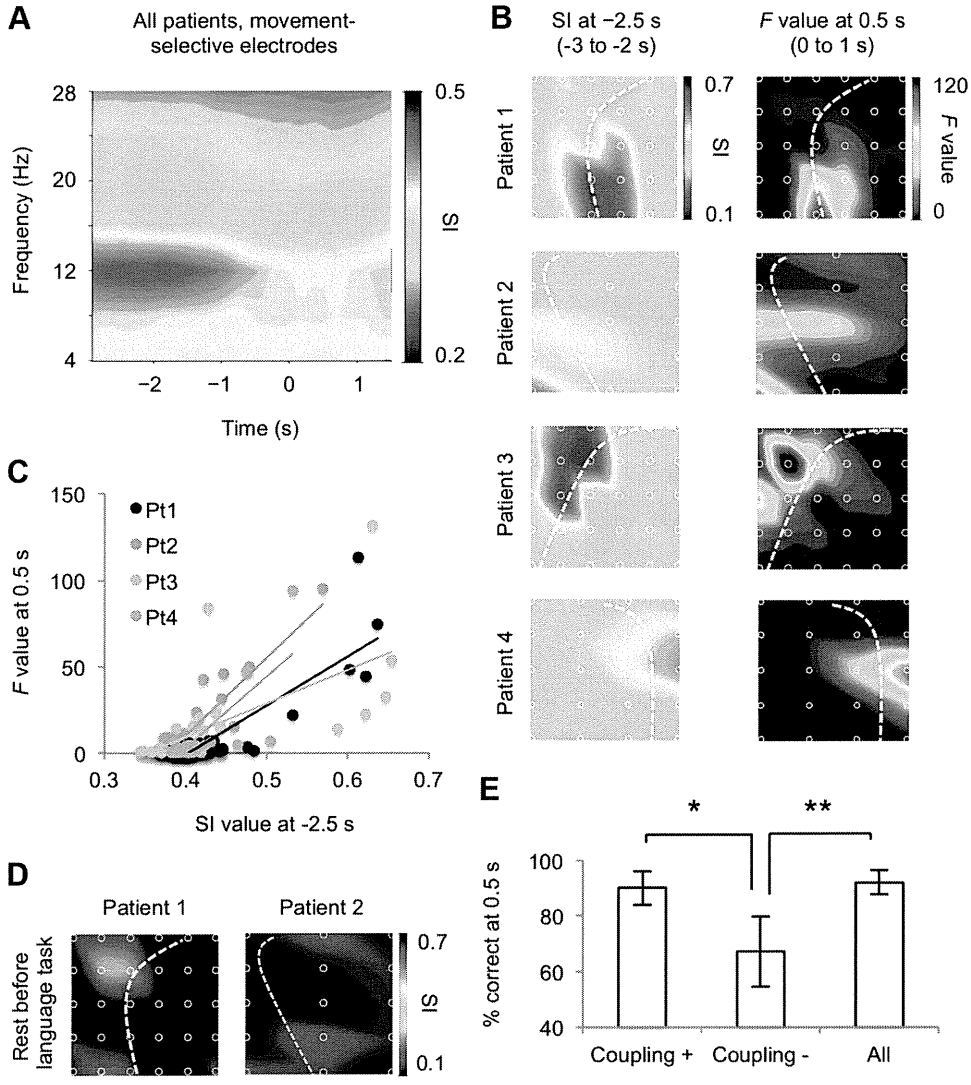

Figure 3. High-γ amplitude during the waiting period was coupled with the α phase at movement-selective cortical areas. ***A***, Significant SI values between the high-γ amplitude and each low-frequency phase (2–30 Hz, 4 Hz width) of 1 s intervals centered at every 100 ms were averaged across the movement-selective electrodes of all patients. The mean SI value was color-coded at each time and low-frequency band. ***B***, The mean SI value at −2.5 s (−3 to −2 s) (Left) and the *F* value at 0.5 s (Right) are color-coded to the location of the electrodes for each patient. ***C***, The mean SI values at −2.5 s and the *F* values at 0.5 s for each electrode are shown for each patient. Each color corresponds to each patient. ***D***, The mean SI values during the resting period of the language task are color-coded to the location of the electrodes for patients 1 and 2. ***E***, The classification accuracy using the mean normalized high-γ amplitude of 1 s intervals centered at 0.5 s was compared among three groups of electrodes (*$p < 0.05$, **$p < 0.01$; error bar, 95% CI). Coupling (+): electrodes with significant SI values at −2.5 s, Coupling (−): electrodes without significant SI values at −2.5 s. All, All electrodes.

confirm that the movement types are represented by high-γ amplitudes around the timing of motor execution (Yanagisawa et al., 2012).

The movement selectivity of the high-γ amplitudes varied among the electrodes. Figure 2*C* shows *F* values (one-way ANOVA *F* statistic) that compute the variability of the high-γ amplitudes across movement types relative to the trial-by-trial variability within movement types at each electrode and patient, and thus quantify the selectivity to movement types. Only a subset of electrodes showed high *F* values (movement selectivity), and all patients showed different spatial patterns of *F* values across electrodes. In the following analyses, we focus, though not exclusively, on the electrodes with high movement selectivity with *F* values of $p < 0.01$ (one-way ANOVA) at 0.5 s. We call them "movement-selective electrodes" or "movement-selective cortical areas."

Figure 2*D* shows an example of high-γ signals at a movement-selective electrode of patient 1. The high-γ signals increased or decreased around the timing of motor execution depending on the movement type, while the high-γ amplitude during the waiting period (>2 s before execution) was not selective to the movement type. It should be noted that the high-γ amplitudes were not zero even during the waiting period. This can also be seen in Figure 2*A* in which a substantial amount of high-γ activity was found during the waiting period, though not as pronounced as during the execution period. This led us to characterize high-γ activity during the waiting period.

High-γ amplitude during waiting is coupled with the α phase at movement-selective cortical areas

To characterize high-γ activity during waiting, we performed PAC analysis using the SI. At each movement-selective electrode, we calculated the SI value between the high-γ amplitude and the phase of the low-frequency bands (2-30 Hz, 4 Hz width). Figure 3*A* shows the SI values at each coupling frequency and timing averaged across the movement-selective electrodes of all subjects.

High SI values were found at the α phase (10–14 Hz) during the waiting period (>2 s before execution), indicating that high-γ activity during waiting is strongly coupled with the α phase ($p < 0.01$, ANOVA).

We next examined the distribution of the SI values between the high-γ amplitude and α phase (10–14 Hz) across electrodes during waiting. Interestingly, the spatial pattern of the SI values at −2.5 s (−3 to −2 s, waiting) in each patient (Fig. 3*B*, left) look similar to that of the *F* values at 0.5 s (0–1 s, execution; Fig. 3*B*, right), which indicate movement selectivity. Figure 3*C* shows the SI values at −2.5 s and *F* values at 0.5 s at each electrode and patient. The scatter plot reveals a high correlation between SI and *F* (correlation coefficients for patients 1-4, 0.85, 0.90, 0.63, and 0.73, respectively; $p < 0.01$ for all, corrected for multiple comparison). Notably, the distribution of the SI values was not the same in different tasks. For example, during the waiting period before the language task in which patients 1 and 2 were asked to voluntarily pronounce some Japanese vowels, the SI values were not correlated to the *F* values at 0.5 s for the movement tasks (correlation coefficients for patients 1 and 2, 0.07 and 0.09, respectively). These results suggest that the coupling of high-γ activity with the α phase during waiting for movement is restricted in the movement-selective area with movement-selective high-γ activity during execution.

The high correlation between the SI at waiting and *F* at execution allows us to select effective electrodes for multichannel decoding. We divided the electrodes into two groups: electrodes with significant SI values at −2.5 s (Coupling (+)) and others (Coupling (-)). The significance was defined by a *t* test comparing the mean SI values with an unshuffled and shuffled α phase ($p < 0.05$). Multichannel decoding analysis using high-γ amplitudes at 0.5 s revealed that the decoding accuracy of Coupling (+) was significantly higher than that of Coupling (-) ($p < 0.05$ corrected for multiple comparison, *t* test), and was comparable to the performance using all electrodes (Fig. 3*D*). This finding further confirms that PAC during waiting signals movement-selective cortical areas.

High-γ amplitude at movement-selective areas peaks around the trough of the α oscillation during waiting

To further characterize the coupling between the α phase and the high-γ amplitude, we plotted the time courses of SI and α amplitudes averaged across trials, movement-selective electrodes, and patients. The SI value was largest at −1.7 s and gradually decreased toward the timing of motor execution ($p < 0.01$, ANOVA; Fig. 4*A*). The α amplitude followed a similar time course ($p < 0.01$, ANOVA), suggesting that the coupling of the high-γ amplitude is modulated by the amplitude of the α oscillation. It should be noted that the SI is independent of the amplitude of the frequency component defining the phase (α in this case), although in noisy conditions, low signal amplitudes could lead to a poor phase estimation resulting in small SI values. Our simulation using synthetic α and high-γ oscillations with added noise confirmed that when the α amplitude was varied, the SI remained constant at all amplitudes except at extremely low amplitudes (data not shown). Therefore, the similarity of the time courses of the SI and α amplitude is unlikely to be an artifact arising from the definition of the SI and the signal-to-noise-ratio.

While the SI quantifies the "strength" of PAC, it does not indicate with which phase the amplitude is coupled. To reveal the α phase at which high-γ activity is enhanced, we calculated the high-γ amplitude and α phase at −2.5 s in each trial using the movement-selective electrodes, and averaged the high-γ amplitudes within each of the 6 bins of the α phase (60° width). We found that the α phase-conditioned high-γ amplitudes varied significantly among the phase bins ($p = 0.019$, one-way ANOVA), and that strong high-γ activity was observed at the trough of the α oscillation (180° ± 30°; Fig. 4*B*, left). When the same analysis was performed at 0.5 s, the α phase-conditioned high-γ amplitudes were not significantly different across the α phase bins ($p = 0.998$, ANOVA; Fig. 4*B*, right).

PAC does not represent movement type

We have seen that the high-γ amplitudes during waiting are not selective to, and not predictive of, movement type (Fig. 2), while the strength of PAC during waiting in each electrode is correlated with the movement-selectivity during execution. However, it is still possible that the ECoG features associated with PAC during waiting may be selective to or predictive of movement type. To test this, we examined the spatial patterns of (1) the SI values and (2) the phase differences between α and the α component of high-γ amplitude modulation ($\phi_\alpha[t] - \phi_{\gamma\alpha}[t]$) for each movement type and performed multielectrode decoding using these as input features. Figure 5*A* illustrates an example of the SI values and phase differences of patient 1 at −2.5 s. The spatial distribution of the SI values and phase differences did not show a clear difference across the movement types. Decoding accuracy was close to the chance level during both the waiting and execution periods in all patients (Fig. 5*B*). It should be noted that our experimental design did not control the timing of when the patient decides to perform the movement type. Therefore, the failure to decode movement types early in the waiting period could simply be due to the fact that the decision was not made yet. These results suggest that PAC does not directly represent movement types while modulating high-γ amplitudes in movement-selective areas independently of movement type.

Hold-and-release regulation of the high-γ amplitude by PAC

Finally, we characterized the dynamics of high-γ activity throughout a movement trial using phase-conditioned plots. Figure 6*A* shows examples of the time courses of α phase-conditioned high-γ amplitudes (six phase bins) averaged within each movement type (for one electrode with the highest *F* value in each patient). During the waiting period, α phase-conditioned high-γ activity showed varying amplitudes across the phase bins with high amplitude in the 180° bin. However, toward the timing of motor execution, the high-γ activity of all phases converged on three different values depending on the movement type. This time course of high-γ activity is consistent with the results shown in Figure 4*B*. Figure 6*B* shows *F* (movement selectivity) and SI (strength of PAC) values averaged across the movement-selective electrodes of four patients. Movement selectivity (*F*) appeared to arise when PAC (SI) was attenuated for all phase bins. A negative correlation between the *F* and SI values was found in the data averaged across all subjects and movement-selective electrodes (correlation coefficients for all phase bins $r < -0.7$). Interestingly, while the spatial distributions (across electrodes) of the *F* values during execution and SI values during waiting were positively correlated (Fig. 3), the *F* and SI values were negatively correlated in the time domain. These results suggest that while PAC occurs during the waiting period only at movement-selective areas, it modulates high-γ activity to hold the amplitude at a fixed state during waiting, and then to release it to movement-specific states.

Discussion

In the current study, we explored PAC on the sensorimotor cortex and its relation to the motor representation by the high-γ amplitude. The high-γ amplitudes in the movement-selective electrodes were shown to be strongly coupled with the α phase during the waiting period for the movement task. The coupling held the high-γ amplitude at the phase-dependent status in which the amplitude did not represent the movement type. While the coupling was attenuated toward the execution of the movements, the high-γ amplitude was released from the phase-dependent status to have some particular values depending on the movement type. The strength of the coupling was negatively correlated with the movement-selectivity of high-γ activity along the time course of the task. These results support the idea that PAC on the sensorimotor cortex critically affected the behavior of the high-γ amplitude to modulate the motor representation.

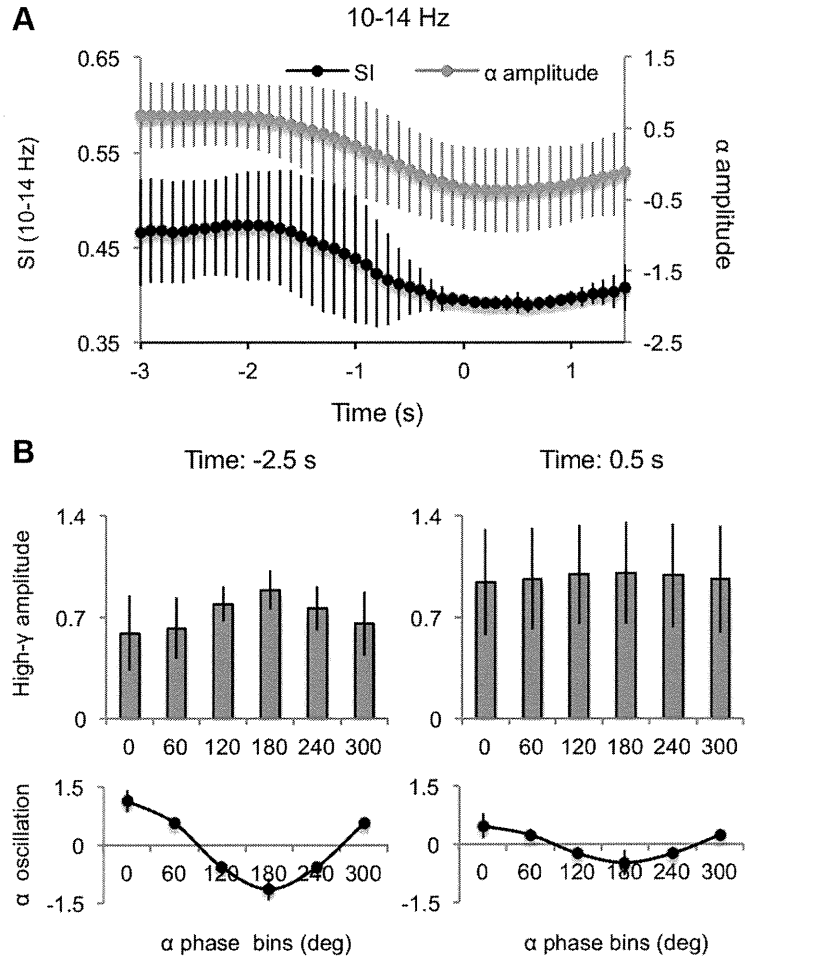

Figure 4. High-γ amplitude during waiting peaked around the trough of the α oscillation. ***A***, The mean SI value and the mean α amplitude of all trials were averaged among the movement-selective electrodes of four patients (error bar, 95% CI). The averaged SI value and the averaged α amplitude were significantly decreased during the execution of the movements ($p < 0.01$, one-way ANOVA). ***B***, Top, The high-γ amplitudes were averaged over each of the 6 phase intervals of 10–14 Hz oscillations for 1 s intervals centered at −2.5 s or 0.5 s of all trials (α phase-conditioned high-γ amplitude). The α phase-conditioned high-γ amplitudes were averaged across the movement-selective electrodes of four patients at each time (error bar, 95% CI). The α phase-conditioned high-γ amplitudes varied significantly among the 6 phase intervals at −2.5 s ($p = 0.019$, one-way ANOVA), though not significant at 0.5 s ($p = 0.998$, one-way ANOVA). Bottom, The α oscillation, which was the ECoG signals bandpass filtered at 10–14 Hz, was averaged over each of the 6 phase intervals of 10–14 Hz oscillation for 1 s intervals centered at −2.5 s (left) or 0.5 s (right) of all trials. The α oscillations were averaged among the movement-selective electrodes of four patients at each time (error bar, 95% CI).

Hold-and-release model of high-γ amplitude

We found that the large high-γ amplitude was locked to the trough of the α oscillation (10–14 Hz) before hand movements. Recently, it was shown that neuronal spiking on the sensorimotor cortex was locked to the trough of the α oscillation (8–14 Hz) on the sensorimotor cortex during a vibrotactile discrimination task (Haegens et al., 2011b). Our finding is consistent with this observation because the high-γ amplitude has been shown to be correlated with the firing rate (Ray et al., 2008; Quian Quiroga and Panzeri, 2009). The PAC between the high-γ amplitude and the α phase might reflect a local mechanism in which neuronal firing is modulated by the ongoing α oscillation (Klimesch et al., 2007; Mathewson et al., 2011). Notably, previous studies on phase-amplitude coupling of α oscillation has mostly focused on the visual/sensory domain, while our study demonstrated that the coupling and related neuronal processing can be extended to the motor domain (Haegens et al., 2011b; Jensen et al., 2012).

Here, we provided an insight into how the motor representation by the high-γ amplitude was modulated by the α oscillation through PAC. It was demonstrated that PAC inhibited the motor representation by restricting the high-γ amplitude in the phase-dependent state. The coupling was strong at the movement-selective cortical areas and diminished with the attenuation of the α amplitude to hold-and-release the high-γ amplitude. Some previous studies have suggested that the attenuation of α oscillation facilitates processing in task-relevant cortical regions to improve task performance, whereas increased α oscillation suppresses distracting input in task-irrelevant regions (Palva and Palva, 2007; Mazaheri and Jensen, 2010; Gould et al., 2011; Haegens et al., 2011a,b). These findings are consistent with our results showing that the strong coupling with larger α oscillation suppresses cortical processing by restricting the high-γ amplitude and that the attenuation of the coupling with smaller α oscillation facilitates motor representation by releasing the high-γ amplitude. Since the coupling during the waiting period was limited to the electrodes showing high movement selectivity during motor execution, the α oscillation may selectively hold-and-release the high-γ amplitude at the movement-selective regions to modulate motor representation.

Functional roles of PAC during preparation

The functional roles of PAC have been a matter of speculation. In some previous studies, PAC has been shown to have a variety of functional roles in various cortical regions, such as working memory in the hippocampus (Axmacher et al., 2010) and sensory processing in the auditory cortex, primary visual cortex and primary motor cortex (Luo and Poeppel, 2007; Lakatos et al., 2008; Saleh et al., 2010). Although the functional role of the coupling in

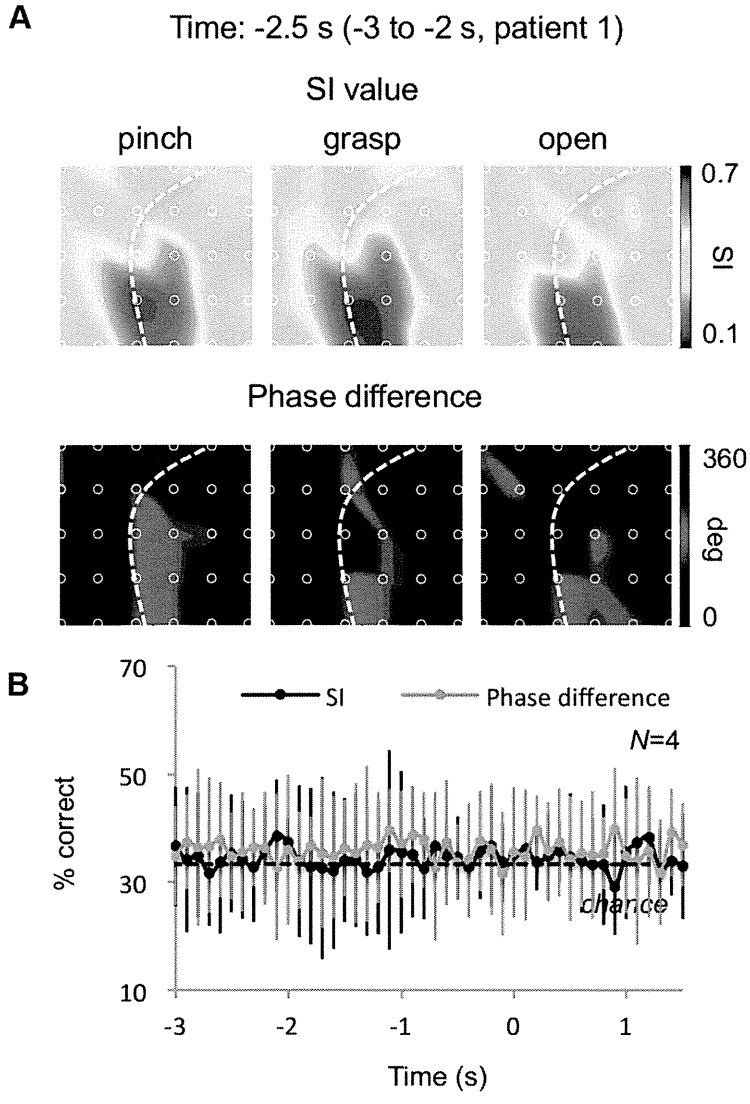

Figure 5. PAC did not represent movement type. ***A***, The SI value and the phase difference of each electrode were averaged over a 1 s interval centered at −2.5 s for each of the three types of movement of patient 1. The mean SI value and the phase differences were color-coded to the location of the electrode. ***B***, The percentage correct of the movement classifications using the spatial distribution of the mean SI value or the mean phase difference of 1 s intervals centered at every 100 ms was averaged among 4 patients (error bar, 95% CI). The dotted line shows the chance-level accuracy of 33.3%.

the sensorimotor cortex has not been elucidated, some previous studies have shown that low-frequency oscillations are related to the performance of movement tasks and maintenance of the status quo (Gilbertson et al., 2005; Engel and Fries, 2010; Haegens et al., 2011b). The coupling might contribute to these functions by modulating the high-γ amplitude.

Our results revealed that the high-γ amplitude was activated at the trough of the α oscillation even before the movements, although the mean high-γ amplitude was small. The high-γ amplitude on a particular α phase might contribute to control muscle contractions for the maintenance of the status quo. Furthermore, the coupling might be related to the preparation of movements without sufficient information of the actual movement type. Recently, it was shown that neural activity for the preparation of movements was not simply a subthreshold form of movement activity and provided the initial state of a dynamic system whose evolution produced movement activity (Churchland et al., 2010). The strong PAC might provide the initial state for the activation of the high-γ amplitude to represent the motor information.

In previous studies, the maintenance of the status quo has often been attributed to β rhythms (Engel and Fries, 2010). In additional analysis, we examined the functional similarity between the PAC and β activity by calculating the correlation coefficient between the spatial distributions of the β amplitudes (22–26 Hz) during the waiting period and the F values of high-γ amplitudes during execution (Fig. 3*C*; except that the SI values were replaced with β amplitudes, as). We did not find consistently high correlations between the β amplitudes and the F values across the patients (patients 1–4: 0.14, 0.63, −0.27, −0.06, respectively), in contrast to the consistently high correlations between the SI and F values (patients 1–4: 0.85, 0.90, 0.63, 0.73, respectively; Fig. 3*C*). Thus, the β amplitude was not selectively activated in the movement-selective cortical regions in most patients. These observations suggest that PAC serves more localized functions in motor preparation than β activity. However, it should be noted that although we focused on the PAC of the α range, high SI values before movements were not limited to the α range, but also extended over the β range (Fig. 3*A*). Therefore, β oscillations, together with α oscillations, may be involved in spatially localized functions in motor preparation via PAC with high-γ oscillations.

High-γ amplitude was coupled with the α/μ phase in the sensorimotor cortex

PAC has been observed across multiple cortical areas under a variety of experimental conditions in humans (Bruns and Eckhorn, 2004; Vanhatalo et al., 2004; Mormann et al., 2005; Pineda, 2005; Canolty et al., 2006; Osipova et al., 2008; Cohen et al., 2009; Händel and Haarmeier, 2009; Axmacher et al., 2010; He et al., 2010; Sadaghiani et al., 2010). Notably, the dominant low-frequency rhythms providing the phase for PAC depend on the region and task. For example, θ–γ coupling was predominant in the anterior frontal and temporal cortices during an auditory task, whereas α-γ coupling was strong over occipital areas during a visual task (Voytek et al., 2010). In addition to these findings, our results have shown that α-γ coupling was predominant in the sensorimotor cortex during a motor task, adding further diversity to PAC. It should be noted that in the human sensorimotor cortex, the α oscillation is also known as the μ rhythm, which is characterized by large amplitudes before movements and attenuation during movements (Sabate et al., 2012).

Implications for brain-machine interfaces

Although our results suggest that the features of PAC are not predictive of future movements, this coupling could be applied to improve brain-machine interfaces (Yanagisawa et al.,